Environmental Science and Pollution Research (2023) 30:8822–8834
https://doi.org/10.1007/s11356-022-21755-0

Removal of Cr(VI) from water by *in natura* and magnetic nanomodified hydroponic lettuce roots

Beatriz Caliman Soares[1] · Thais Eduarda Abilio[1] · Julia Cristina José[1] · Geórgia Labuto[2,3] · Elma Neide Vasconcelos Martins Carrilho[1,4]

Received: 31 October 2021 / Accepted: 26 June 2022 / Published online: 9 July 2022

Abstract

Biosorption is a viable and environmentally friendly process to remove pollutants and species of commercial interest. Biological materials are employed as adsorbents for the retention, removal, or recovery of potentially toxic metals from aqueous matrices. Hexavalent chromium is a potential contaminant commonly used in galvanoplasty and exhibits concerning effects on humans and the environment. The present work used *in natura* lettuce root (LR) and nanomodified lettuce root (LR-NP) for Cr(VI) adsorption from water medium. The nanomodification was performed by coprecipitation of magnetite nanoparticles on LR. All materials were morphologically and chemically characterized. The conditions used in removing Cr(VI) were determined by evaluating the pH at the point of zero charge ($pH_{PZC} = 5.96$ and 6.50 for LR and LR-NP, respectively), pH, kinetics, and sorption capacity in batch procedures. The maximum sorption capacity of these materials was reached at pH 1.0 and 30 min of adsorbent-adsorbate contact time. The pseudo-second-order kinetic equation provided the best adjustments with r^2 0.9982 and 0.9812 for LR and LR-NP, respectively. Experimental sorption capacity (Q_{exp}) results were 4.51 ± 0.04 mg/g, 2.48 ± 0.57 mg/g, and 3.84 ± 0.08 mg/g for LR, NP, and LR-NP, respectively, at a 10 g/L adsorbent dose. Six isothermal models (Langmuir, Freundlich, Sips, Temkin, DR, and Hill) fit the experimental data to describe the adsorption process. Freundlich best fit the experimental data suggesting physisorption. Despite showing slightly lower Q_{exp} than LR, LR-NP provides a feasible manner to remove the Cr(VI)-containing biosorbent from the medium after sorption given its magnetic characteristic.

Keywords Biosorption · Biomass · Water treatment · Magnetite nanoparticles · Hexavalent chromium

Introduction

The growing industrialization is a substantial cause of environmental degradation, mainly by disposing contaminated effluents inappropriately (Dhankhar and Hooda 2011). The discarding of effluents with no prior treatment results in the introduction of pollutants such as potentially toxic metals, dyes, and drug residues, which are harmful to human health and aquatic fauna, causing mortality of species existing in these ecosystems (Santos et al. 2011).

Among the most harmful contaminants are toxic metals, which can be a severe environmental and health risk when present in concentrations higher than legally permitted. Metals are not biodegradable and can be a health risk due to their toxicity and carcinogenicity. Several anthropogenic sources introduce chromium, a very rigid toxic metal in the environment (Rossi et al. 2018; Jobby et al. 2018).

Communicated by Tito Roberto Cadaval Jr.

✉ Elma Neide Vasconcelos Martins Carrilho
elma.carrilho@gmail.com

[1] Laboratory of Polymeric Materials and Biosorbents, Universidade Federal de São Carlos, Araras, SP 13600-970, Brazil

[2] Departamento de Química, Universidade Federal de São Paulo, Diadema, SP 09913-030, Brazil

[3] Laboratory of Integrated Sciences, Universidade Federal de São Paulo, Diadema, SP 09913-030, Brazil

[4] Departamento de Ciências da Natureza, Universidade Federal de São Carlos, Matemática e Educação, Araras, SP 13600-970, Brazil

Chromium occurs naturally in the earth, but different from other toxic metals; it shows oxidation states such as Cr^{3+} and Cr^{6+}. These species are directly related to pH and redox conditions in the aqueous phase. Hexavalent chromium is its most toxic form, which is not found naturally in water but ends up being mainly discharged through effluents from steel industries (Conceição et al. 2014; Kanagaraj and Elango 2019). A high concentration of hexavalent chromium causes lung and stomach cancer, diabetes, and nasal cavity, different from Cr(III), which is an essential micronutrient for humans (Kanagaraj and Elango 2019). Due to the severe consequences of Cr(VI) in water, several treatment methods have been proposed for its removal. Although conventional wastewater treatment methods (chemical precipitation, flocculation, ion exchange, and filtration) are still employed, their application presents various limitations. They are not economically feasible, require a long time to be implemented, and are not doable if contaminants are found in large volumes of water (Santos et al. 2011; Babu et al. 2019). Among the alternatives for removing pollutants from the environment, biosorption, a physicochemical process started in the early 1970s, has been proposed and differs from other methods due to its low cost and high efficiency (Abilio et al. 2021; Carvalho et al. 2021; Cid et al. 2020; Gadd 2009). Biomass retains contaminants on the surface due to the active sites available in its composition and can uptake cations and anions by physicochemical interaction occurring between adsorbate and adsorbent. Biosorption consists of the use of biomasses from biological materials, such as hydroponic lettuce root, a widely available residue with no economic relevance. Previous studies using *in natura* and chemically modified hydroponic lettuce roots demonstrated their potential as adsorbents for the removal of Cu(II), Fe(II), Zn(II), and Mn(II) (Milani et al. 2018a, 2018b).

Lettuce is a widely consumed vegetable. In 2005, world lettuce production was 22 million tons, and it is mainly cultivated in temperate and subtropical regions (Mou 2008). This vegetable grows a deep taproot with horizontal lateral roots near the soil and water, absorbing water and nutrients (Mou 2008). For this reason, lettuce roots are promising biomass to be used as biosorbents due to the presence of cellulose, hemicellulose, and proteins (Akhter et al. 2014).

Some techniques can be employed to improve and facilitate the biosorption process or increase the sorption capacity of the material, such as the use of magnetic nanoparticles. Due to the small sizes of these materials, which range from 1 to 100 nm, they have properties that cause repulsive and attractive interactions with the magnetic field and can be easily removed from the medium with the use of a magnet after the sorption process (José et al. 2019; Debs et al. 2019; Labuto et al. 2018).

Given the incorrect disposal of wastewater containing emerging contaminants, such as potentially toxic metals, it is necessary to think of ways to remedy these ecosystems, to reduce the damage to living beings. Chromium(VI) is a toxic metal and exhibits carcinogenic effects. Its emission comes mainly from leather tanning, chromate production, paint manufacturing, and electroplating (ARIF et al. 2020). The use of lettuce roots as biosorbents for Cr(VI) in its removal is a new approach since this material has not yet been used. Therefore, this work proposes this environmentally friendly, promising, and economically viable alternative to treat Cr(VI)-contaminated water. In addition, nanomodification of the roots' biomass facilitates the removal of the adsorbent from the medium after the adsorption process. In this way, this research contemplates significant aspects of this biomass potential that has not been previously reported.

The aim of this work is to prepare *in natura* and nanomodified hydroponic lettuce roots from domestic and agro-industrial residues and use them for the removal of Cr(VI) species in the aqueous medium, as a promising alternative for water and effluent remediation.

Material and methods

Reagents and samples

All solutions used in this work were prepared using deionized water obtained from a Direct-Q 3 System (Merck Millipore, Germany). The buffer solution at pH 5.5 was prepared from 100% glacial acetic acid and potassium acetate dilutions to obtain a 0.005 mol/L KCH_3COO/CH_3COOH (Synth, São Paulo-SP, Brazil) solution. The Cr(VI) stock solution was prepared by dissolving $K_2Cr_2O_7$ (LabSynth, São Paulo, Brazil) in deionized water. The magnetic materials were prepared with $FeCl_3{\cdot}6H_2O$, $FeSO_4{\cdot}7H_2O$, HCl, and NH_4OH, and ethanol was used to wash the obtained nanomaterials (all from LabSynth, São Paulo-SP, Brazil). Hydrochloric acid, NaOH, and NaCl (Synth, São Paulo-SP, Brazil) were used in the *pH assessment point of zero charge* (pH_{PZC}) determination procedure.

The hydroponic lettuce root biomass used in the present work was produced in the Federal University of São Carlos (Araras-SP, Brazil). This material was washed with distilled deionized water for the total removal of solid residues. After washing, the material was oven-dried (Te-394/1, Tecnal Scientific, Piracicaba-SP), ground in a rotor mill, passed through a 0.12-mm sieve, and stored.

Synthesis of Fe_3O_4 nanoparticles and the magnetic bionanocomposite (LR-NP)

A coprecipitation method (Panneerselvam et al. 2011; Cardona et al. 2019) was used to synthesize magnetite

nanoparticles (NPs) and the magnetic nanomodified lettuce root (LR-NP) biomass. The procedure consists of the dissolution of Fe(II) and Fe(III) salts at a 1:2 molar ratio, respectively, in a 1.0 mol/L HCl medium. Under constant stirring, 0.7 mol/L NH_4OH was slowly added to this solution for about 30 min. After this synthesis, the *in natura* lettuce root (LR) was added to the synthesized NP at a 5:1 ratio, respectively, according to Abilio et al. (2021), under constant heating and stirring to prepare the nanocomposite LR-NP. Reactions 1 and 2 demonstrate the synthesis of NP and LR-NP, respectively.

$$Fe^{2+}_{(aq)} + 2Fe^{3+}_{(aq)} + 8OH^{-}_{(aq)} \rightarrow Fe_3O_{4(s)} + 4H_2O_{(l)} \quad \text{(Reaction 1)}$$

$$Fe_3O_{4(s)} + LR_{(s)} \rightarrow LR - Fe_3O_{4(s)} \quad \text{(Reaction 2)}$$

Characterization of LR, NP, and LR-NP

All materials were characterized by Fourier transform infrared spectroscopy (FTIR, Bruker, Vertex Model), scanning electron microscopy (ZEISS LEO 440 with OXFORD detector 7060 model), and X-ray diffraction (XRD, Rigaku MiniFlex 600 Model). FTIR analysis was used to identify functional groups responsible for toxic metal removal present in the surface of the biosorbent (Babu et al. 2019). The equipment operated with 32 scanners ranging from 4000 to 400 cm^{-1}, using pellets made with the samples and potassium bromide.

Scanning electron microscope (SEM) analysis was carried out to obtain external images of the material's surface. It operated with a 10-kV electron beam, 2.82-A current, and 200-pA probe. The samples were carbon-coated in a BAL-TEC MED 020 Coating System metallizer (BAL-TEC, Liechtenstein) and desiccated until analysis.

The X-ray diffraction analysis allows determining the crystalline structures present in the materials. A powder X-ray diffractometer equipped with a copper X-ray source (CuKα tube) was used with λ = 1.5406 Å, 40-kV voltage, and 30-mA current. Data were obtained in the range of 2° to 90° at a rate of 0.02° per second.

pH assessment: point of zero charge and sorption pH

The pH_{PZC} is the pH in which the charge of the biosorbent surface is electrically zero. The material is positively charged when exposed to a solution at pH below the pH_{PZC}. If the solution is at a pH greater than pH_{PZC}, the material's surface will be negatively charged. It allows to predict the material surface charge and conduct the adsorption assays under a more suitable condition for the adsorption process (Bakatula et al. 2018; Brito et al. 2019). Thus, it is possible to get the best pH values to perform adsorption.

Firstly, 0.1 mol/L NaCl solutions with initial pH values ranging from 2.0 to 12.0 were added to LR or LR-NP at a 1.0 g/L dosage. The suspensions were left under constant stirring at 185 rpm for 24 h, after which the final pH was measured.

After the pH_{PZC} determination, pH assessment was performed with pH values ranging from 1.0 to 6.0 for LR and 1.0 to 6 for LR-NP, using HCl or NaOH 1 mol/L to adjust Cr(VI) solutions pH. LR and LR-NP at a 25 g/L biosorbent dose were added to Falcon tubes containing 10 mg/L of Cr(VI) solution at different pH values. The suspensions were kept under constant stirring for 10 min at 185 rpm. Using a Nd magnet, the supernatant was separated for further analysis by flame atomic absorption spectrometry (FAAS, AAnalyst 400, PerkinElmer, USA) employing a 1.0 to 6.0 mg/L Cr(VI) calibration curve, and the operating parameters: nebulization flow (5.0 L min/L), air (10.0 L/min), acetylene flow (3.3 L/min), and nebulizer flow rate (2.0 L/min), using a Cr cathode lamp (357.87 nm).

All Cr(VI) sorption assessments (pH, kinetics, and sorption capacity) were performed using batch procedures employing the scheme depicted in Figure S1 available in the Supplementary Material.

Kinetic studies

The kinetic study is significant for optimizing the sorption process, and the procedure is performed by the reaction between adsorbate and adsorbent. The best contact time is when equilibrium is reached. Several kinetic models describe the adsorbate/adsorbent interactions and the adsorption process in the literature. The adjustment is performed according to the kinetic model that best fit the experimental data (Milani et al. 2018b; Raganati et al. 2019).

Two kinetic models were used in the present work: the pseudo-first-order where it assumes that the number of active sites is proportional to the adsorption rate, and the pseudo-second-order, which proposes that the adsorption rate is proportional to the square of the number of active sites present on the adsorbent surface. The mathematical equation of the pseudo-first-order is represented in Eq. 1 (Ho 2006; Raganati et al. 2019).

$$ln(q_e - q_t) = ln(q_e) - k_1 \cdot t \quad (1)$$

where k_1 is the constant of pseudo-first-order (min^{-1}); q_e is the sorption capacities in equilibrium (mg/g); q_t is the sorption capacity at a given time of equilibrium (mg/g); t is the sorption time (min).

Furthermore, the linear equation for the pseudo-second-order is represented in Eq. 2 (Ho and Mckay 2000).

$$\frac{t}{q_t} = \frac{1}{k_2 {q_e}^2} + \frac{t}{q_e}.t \quad (2)$$

where k_2 is the constant of pseudo-second-order (g/(mg/min)); q_e is the mass of adsorbate per gram of adsorbent in equilibrium (mg/g); q_t is the mass of adsorbate per gram of adsorbent in equilibrium, at a given time (mg/g); and t is the sorption time (min).

The kinetics approach was performed using a 10 mg/L Cr(VI) solution with the previously optimized pH = 1.0 and the biosorbents LR or LR-NP at a 10 g/L dosage. The suspensions were kept under constant stirring at 185 rpm using 5, 10, 15, 20, 25, 30, 60, 90, 120, and 150 min contact time between adsorbate and adsorbent. The supernatants were analyzed for Cr determination by FAAS under the previously described operational conditions. This procedure was performed in triplicate.

Sorption capacity and isotherm model parameters

Chromium(VI) solutions were prepared at increasing concentrations (10 to 100 mg/L) at a previously optimized pH value. The solutions were mixed with LR, NP, and LR-NP at a 10 g/L adsorbent dosage. The suspensions were kept under stirring (185 rpm) for 30 min at the best sorption pH (1.0). Thus, the supernatants were removed and analyzed by FAAS to determine the remaining Cr contents under the same conditions previously described in the pH assessment section.

In the experimental sorption capacity assessments, the amount of Cr adsorbed for each concentration (Q_e) was calculated after reaching equilibrium. It was determined by Eq. 3, taking into account Cr concentration in the work solutions before and after sorption, the adsorbent mass, and the adsorbate volume (José et al. 2019).

$$Q_e = \frac{(C_0 - C_e)V}{m} \quad (3)$$

where Q_e is the concentration of adsorbed Cr(VI), in equilibrium (mg/g); C_0 is the initial Cr(VI) concentration (mg/L); C_e is the Cr(VI) concentration in solution, after sorption (mg/L); V is the volume of Cr(VI) solution (L); and m is the biosorbent mass (g).

Six isotherm models, Freundlich, Temkin, Sips, Langmuir, Hill, and D-R, were applied to the experimental data of Cr(VI) sorption to evaluate the best possible adjustment. This analysis correlates the mechanism of adsorption of solutions on solid surfaces with the adsorption isotherm models (Giles et al. 1960). The equations of the non-linear isotherm models used in the current study to assess Cr(VI) sorption by magnetic NPs, LR, and LR-NP, and their respective parameters, are presented in Table S1 (Supplementary Material).

Results and discussion

Characterization of NP, LR, and LR-NP

The FTIR technique was used to identify the main functional groups presented in LR and LR-NP before and after chromium sorption (LR-Cr and LR-NP-Cr). Ferromagnetic nanoparticles (NP and NP-Cr) were also analyzed.

According to the findings in Fig. 1, the prominent bands of functional groups prior to and after sorption are depicted. The prominent peaks in 3400, 2900, 1700, 1250, and 1050 cm^{-1} correspond, respectively, to the asymmetric and symmetric axial deformation of O–H, C–H, C = O, C–O, and C–O–C, mainly attributed to the presence of cellulose and lignin in both LR and LR-NP materials (Silverstein et al. 2012; Milani et al. 2018a).

The infrared spectra of LR and LR-NP prior to and after Cr(VI) sorption exhibited prominent bands around 3200 to 3600 cm^{-1} due to the asymmetric and symmetric axial deformation of alcohols OH, probably from cellulose, hemicellulose, and lignin in the LR biomass, which in the lettuce roots are more evident in this band between 3408 to 3424 cm^{-1} (Mothé and De Miranda 2009). After that, a band between 1722 and 1734 cm^{-1} is observed due to carbonyl groups (C = O) from hemicellulose present in LR. The presence of lignin and cellulose is evident by the asymmetric axial deformation, representing methylene groups (CH_2) and aliphatic and aromatic C–H with symmetry verified at 2927-cm^{-1} absorption (Mothé and De Miranda 2009).

Bands between 1100 and 1200 cm^{-1} are related to hemicellulose and cellulose in LR and LR-NP structures. The

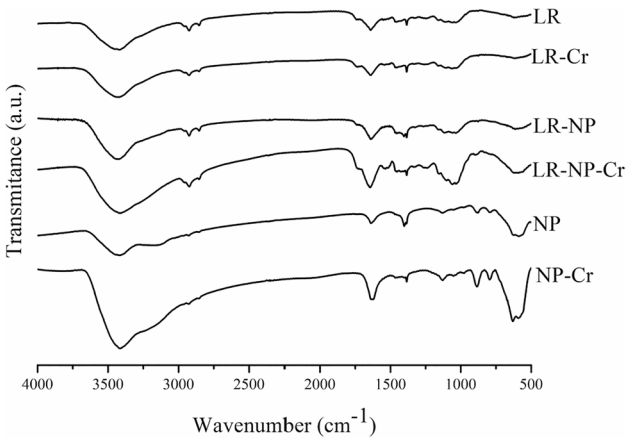

Fig. 1 FTIR spectra of the biomass, nanocomposites, and magnetite in study: lettuce root biomass (LR) prior to and (LR-Cr) after chromium sorption; nanomodified lettuce root biomass (LR-NP) prior to and after (LR-NP-Cr) chromium sorption; magnetite nanoparticles (NPs) prior to and after (NP-Cr) chromium sorption. The spectra are shifted relative to *y*-axis for better viewing

presence of the band deformation in 1024 to 1040 cm^{-1} is due to the bonds of the C–O–C groups of aliphatic and aromatic esters found in the biosorbent (Binod et al. 2012). The band stretching at 1638 to 1645 cm^{-1} after chromium adsorption indicates that aldehydes, esters, and carboxylic acids are involved in the biosorption process (Babu et al. 2018). In addition, some bands were intensified after sorption, possibly related to the availability of Cr(VI) binding sites about 3400 cm^{-1}.

Bands attributed to magnetite are observed at 593 cm^{-1} in the NP infrared spectrum. As predicted, after sorption, the band shifted to 608 cm^{-1} due to the interaction of magnetite with the lignin present in the root biomass, indicating the complete formation and efficient impregnation of NP in LR (Panneerselvam et al. 2011; José et al. 2019).

The micrographs shown in Fig. 2 demonstrate the biomass surface singularities before impregnation and after the nanocomposite formation. According to the literature, the irregular surface observed in LR (2A and 2B) and LR-Cr (2C and 2D) is composed of polysaccharides, pectin, cellulose, and hemicellulose, which contain carboxylic, citric, and malic acids capable of interacting with metallic ions in the aqueous medium (Akhter et al. 2014; Milani et al. 2018b).

The presence of magnetite nanoparticles can be observed on LR surfaces in Fig. 2 before (Fig. 2E, F) and after (Fig. 2G, H) Cr(VI) sorption. It is also noticed that this material exhibits non-uniform particle sizes commonly produced when the coprecipitation method is used and some conglomerates of nanoparticles. As for the nanocomposite SEM, it is possible to observe the root surface covered by Fe_3O_4 prior (Fig. 2I, J) and after (Fig. 2K, L) Cr(VI) sorption. The same fibrous morphology existing in LR and LR-Cr (Fig. 2–D) is also observed, however, with NP's deposition on its surface as indicated in Fig. 2 I–L.

Thus, the images obtained in the morphological analysis of *in natura* and nanomodified lettuce roots (Fig. 2A, B, I, J) show a rough and fibrous aspect with a wide heterogeneous surface area. That favors the use of this material as an ideal biosorbent for removing metal ions from an aqueous medium (Schwantes et al. 2015). In the micrographs obtained to detect the chemical distribution after Cr(VI) sorption (Fig. 2C, D, K, L), it is possible to observe small regions significantly brighter. This observation may imply the occurrence of greater electron backscattering, which coincides with the interaction between the electron beam and heavy metals, such as chromium. This contrast might denote the possible presence of chromium ions on the surface of the biosorbent, being identified when compared with the morphological images before sorption.

In Fig. 3, the diffractograms of nanoparticles and the nanomodified material prior (NP and LR-NP) and after (NP-Cr(VI) and LR-NP-Cr(VI)) sorption are compared to demonstrate the efficiency of the biomass nanomodification with magnetite. As for LR and LR-Cr(VI), no reflection peaks are observed in the diffractograms since LR biomass is composed of organic matter and exhibits an amorphous structure.

Magnetite is chemically composed of ferrous and ferric iron. It is described as iron oxide II and III, and its structure shows an inverted spinel with alternating octahedral and tetrahedral layers. It is possible to observe in its structure that the ferrous species occupies half of the octahedral sites for the possible stabilization of the metal and the ferric species occupy the other half. In addition to this structure, the magnetite unit cell adheres to the face-centered cubic with $a = 0.8396$ nm crystal structure parameter (Blaney 2007). These particularities of the magnetite make it possible to carry out its characterization, generating characteristic peaks due to its inverse spinel structure, the confirmation of biomass impregnation, and the nanoparticle in an efficient manner. The reflection peaks with greater intensities correspond to the planes $2\theta = 30.16°$ (220), 35.5° (311), 43.0° (400), 56.9° (511), and 62.6° (440) (Labuto et al. 2018; Milani et al. 2018a; José et al. 2019; Blaney 2007).

The LR-NP magnetic property observed by the presence of the magnetite crystalline phases and verified by the characteristics of Fe–O stretches in the FTIR analysis is also demonstrated in the images of Fig. 4. This illustration shows the biomass magnetization strength as a neodymium magnet approximates the LR-NP powdered material (Fig. 4B) or an LR-NP-Cr suspension (Fig. 4D). It can be observed that the magnet electromagnetically attracts the nanocomposite to it. This process occurs at about 30 s.

pH assessment: point of zero charge and sorption pH

At the pH_{PZC}, the surface charge of the adsorbents is electrically zero. When exposed to a solution with a pH below the point of zero charge, the material will be positively charged. If the adsorption media is at a pH greater than pH_{PZC}, the surface will be negatively charged (Fernández-Nieves et al. 1998; Zheng et al. 2009; Beretta et al. 2021). Figure 5 depicts the graphical representation of the pH_{PZC} of the adsorbents LR (5.96) and LR-NP (6.50).

If the pH of aqueous solutions is below pH_{PZC}, the material surface is positively charged, showing a cationic form, indicating that the sorption of anionic analytes is favorable. The inverse behavior occurs for the adsorbent material exposed to a value higher than its pH_{PZC}. The material is loaded negatively, indicating an interaction for the sorption of cationic analytes (Appel et al. 2003; Furlan et al. 2010; Gabriel et al. 2021). In aqueous solutions, when exposed to

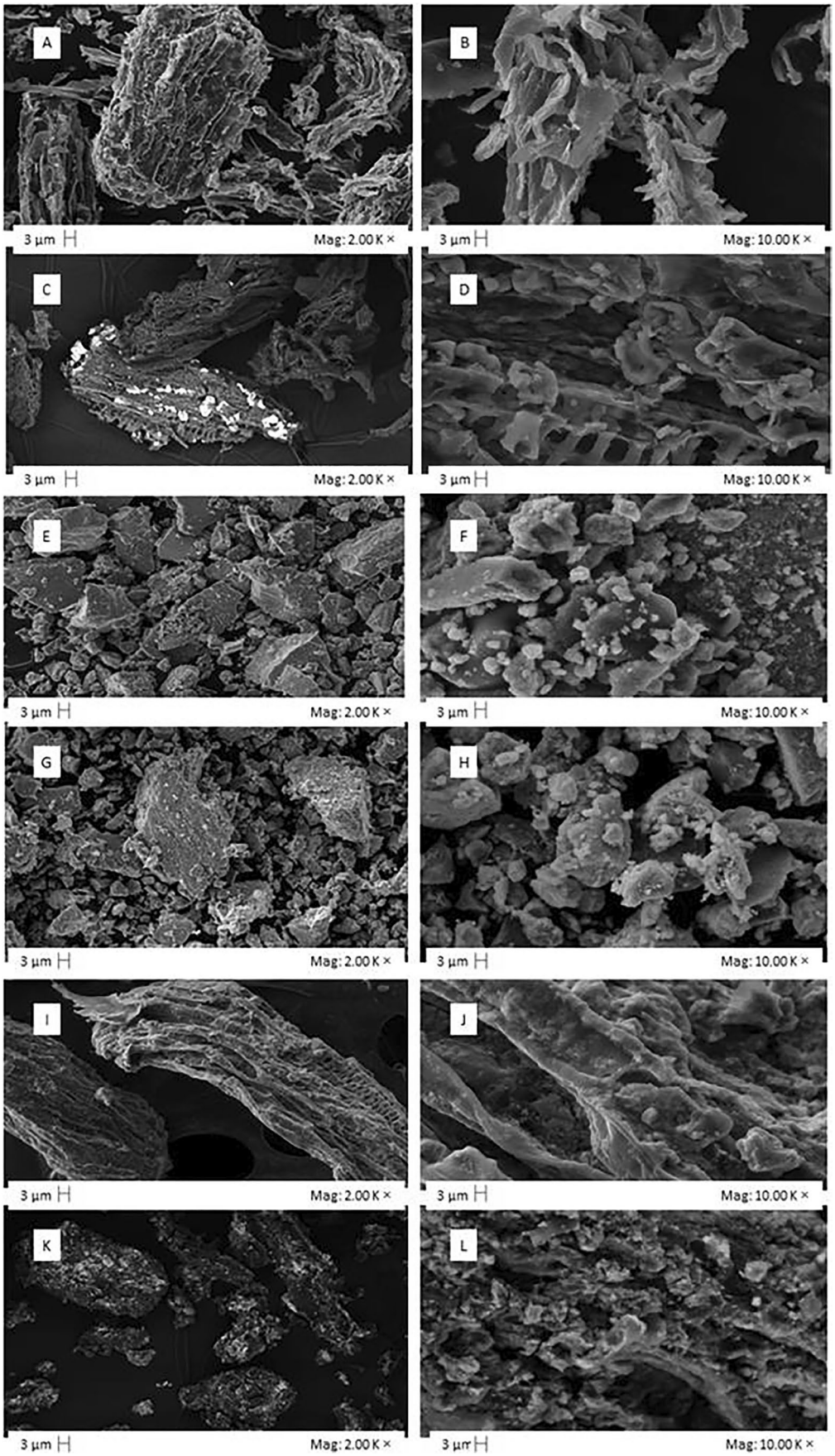
A
3 µm
Mag: 2.00 K ×
B
3 µm
Mag: 10.00 K ×
C
3 µm
Mag: 2.00 K ×
D
3 µm
Mag: 10.00 K ×
E
3 µm
Mag: 2.00 K ×
F
3 µm
Mag: 10.00 K ×
G
3 µm
Mag: 2.00 K ×
H
3 µm
Mag: 10.00 K ×
I
3 µm
Mag: 2.00 K ×
J
3 µm
Mag: 10.00 K ×
K
3 µm
Mag: 2.00 K ×
L
3 µm
Mag: 10.00 K ×

◂**Fig. 2** Scanning electron microscopy (SEM) images of *in natura* lettuce roots (LR) **A**, **B** prior to and **C**, **D** after Cr(VI) sorption; magnetite nanoparticles (NP) **E**, **F** prior to and **G**, **H** after Cr(VI) sorption; nanomodified LR (LR-NP) **I**, **J** prior to and **K**, **L** after Cr(VI) sorption. SEM were obtained at 2 K × and 10 K × magnifications

a pH below pH_{PZC}, Cr(VI) ions are attracted to the surface of lettuce roots and adsorbed as $HCrO4^{-}$.

After determining the pH_{PZC}, the pH effect on the sorption was performed in pH ranging from 1 to 6. The results are presented in Fig. 6. The results indicated that Cr(VI) sorption by LR and LR-NP was favorable below the pH_{PZC}, where the biosorbent surface is positively charged. Above it, the values decreased dramatically. At pH 1.0, both showed the highest efficiency for chromium removal (approximately 86.7% for LR-NP and 87.6% for LR). This behavior was due to the attraction of ions by positively charged functional groups on the surface of the biosorbent.

In aquatic environments, hexavalent chromium can form various species such as CrO_4^{2-}, $HCrO_4^{-}$, and H_2CrO_4, depending on the solution's analyte concentration, pH, and the presence of oxidizing and reducing agents. The predominant chromium species at each pH are presented in Reactions 3 and 4 (Jobby et al. 2018; Omer et al. 2019; Liu et al. 2017).

$$H_2CrO_4 \rightarrow H^+ + HCrO_4^- \ (pH = 1 - 6) \qquad \text{(Reaction 3)}$$

$$HCrO_4^- \rightarrow H^+ + CrO_4^{2-} \ (pH > 7) \qquad \text{(Reaction 4)}$$

The main form of hexavalent chromium in water is the oxyanion. In lower pH values, positive charge is due to functional groups such as amine and hydroxyl protonated at low pH, demonstrating that the strength

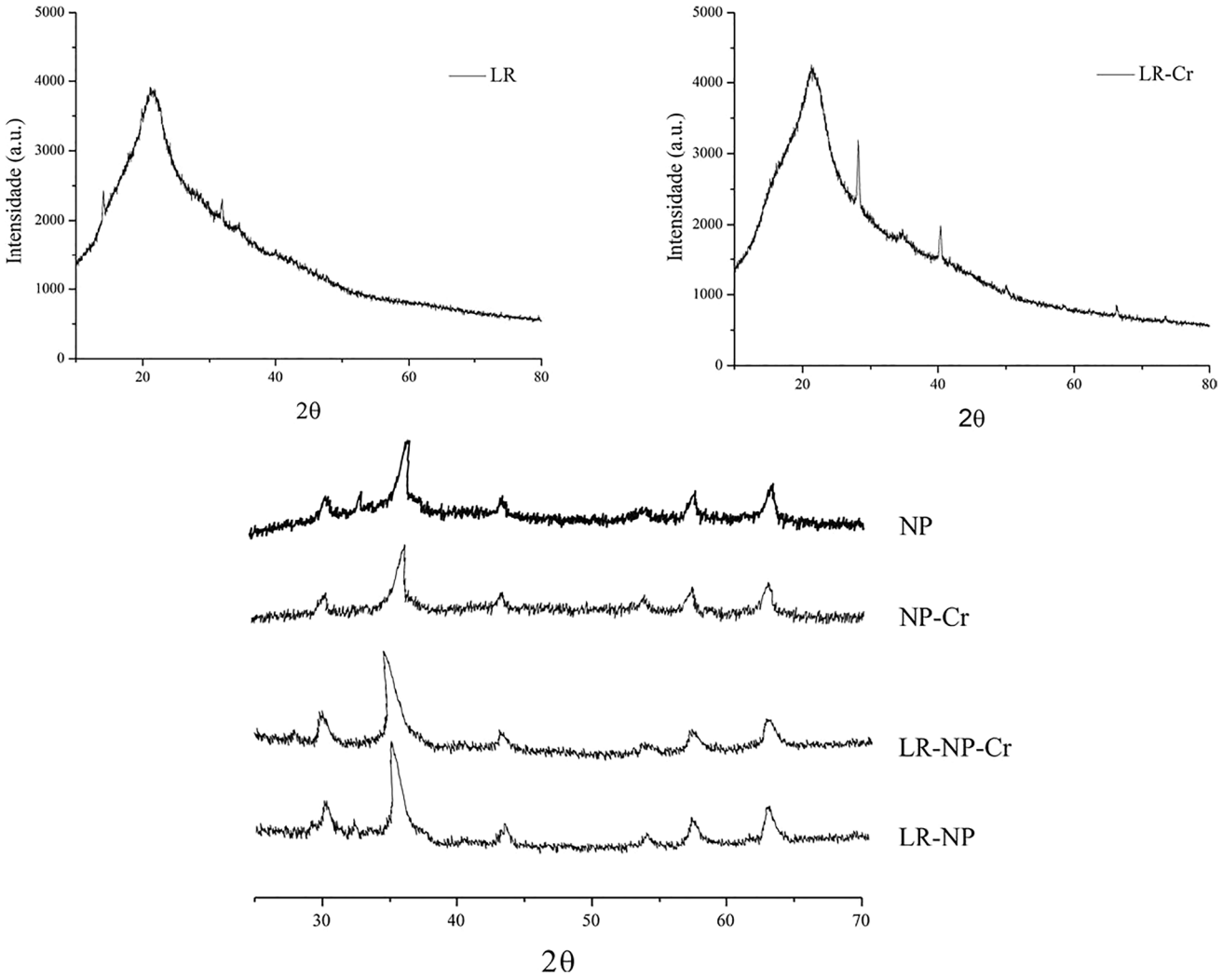

Fig. 3 X-ray diffractograms by magnetic nanoparticle (NP), *in natura* (LR) and nanomodified (LR-NP) lettuce roots prior to and after Cr(VI) sorption

between biomass and the analyte was electrostatic. With the increase in pH, it is observed that adsorption decreases; this consequence is that the degree of protonation decreases and can change to, for example, decreasing electrostatic attraction (Li et al. 2020). This process is described in two ways, the first is through the reduction of Cr(VI) to Cr(III) during the oxidation of organic matter, whereas the second mechanism suggests that the reduction is after adsorption by the surface (Gonzalez et al. 2008; Kratochvil et al. 1998; Yao et al. 2010).

Kinetic studies

The kinetic study results, which indicate the removal of Cr(VI) as a function of the contact time between adsorbent and contaminant at a previously established pH (1.0), are shown in Fig. 7. It is possible to verify that in the first 5 min, chromium retention occurs and that the equilibrium was reached in 30 min for both biosorbents (LR and LR-NP), demonstrating the advantage to use these materials in flow systems for the treatment of effluents.

Table 1 and Figure S2 (Supplementary Material) exhibit the results of the pseudo-first- and pseudo-second-order kinetics models applied to the experimental data.

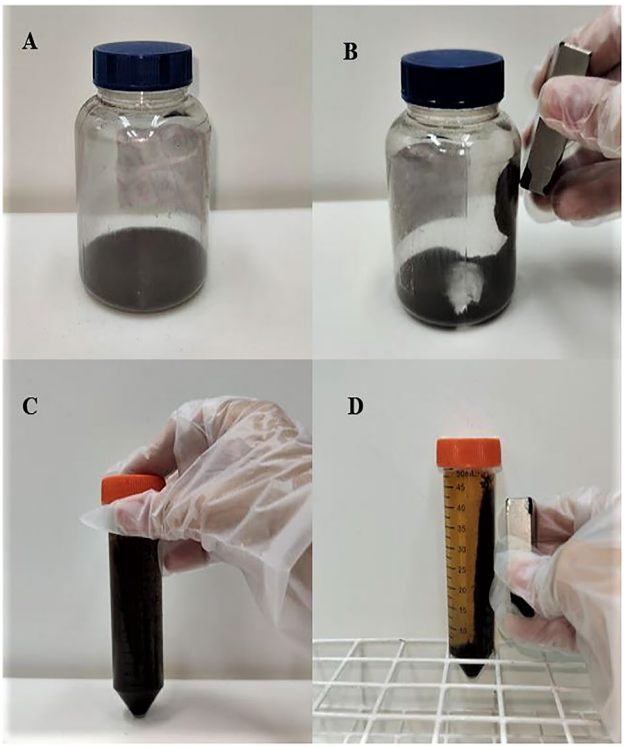

Fig. 4 Illustration of **A** powdered LR-NP nanocomposite and **B** its magnetization effect; LR-NP in Cr(VI) solution **C** prior to and **D** after approximation of a neodymium magnet to this suspension

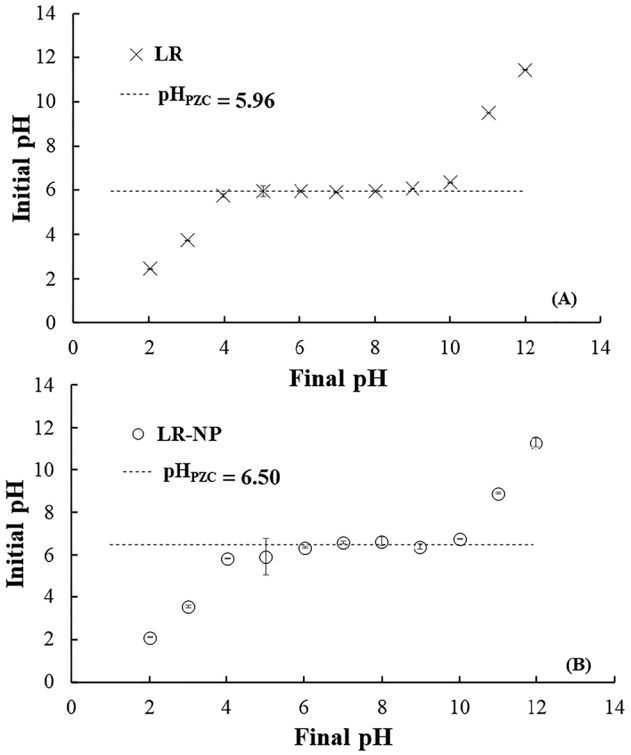

Fig. 5 Point of zero charge (pH_{PZC}) using 1.0 g/L dosage of **A** *in natura* (LR) and **B** nanomodified (LR-NP) lettuce roots with 0.1 mol/L NaCl solution at 2–12 pH range

It is observed that for both materials, LR ($r^2 = 0.9982$) and LR-NP ($r^2 = 0.9812$), the pseudo-second-order equation provided the best fit since their r^2 were close to 1. In addition, this kinetic model was adequate to describe the sorption phenomenon because the Q_e values obtained, 0.523 mg/g for LR and 0.405 mg/g for LR-NP (Table 2), were comparable to those found experimentally for LR

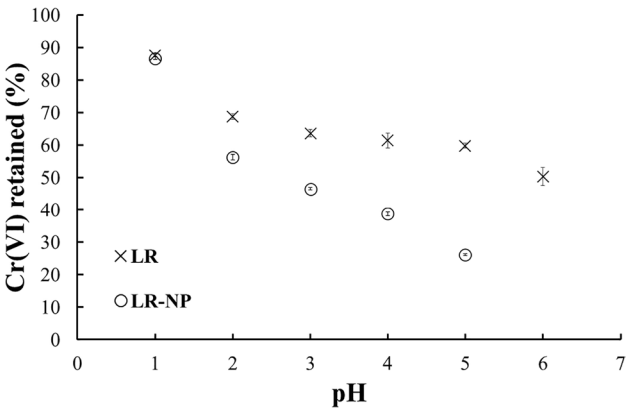

Fig. 6 Effect of pH on Cr(VI) sorption capacity by *in natura* (LR) and nanomodified (LR-NP) lettuce roots, at 10 g/L adsorbent dosage and 10 mg/L Cr(VI) solution. $n = 3$

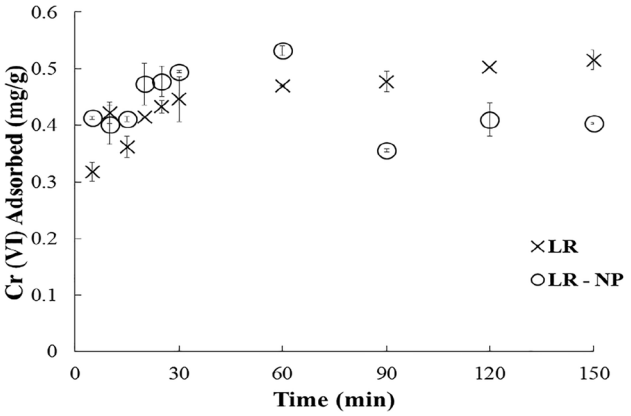

Fig. 7 Cr(VI) sorption kinetics employing 5, 10, 15, 20, 25, 30, 60, 90, 120, and 150 min contact time, 10 g/L dosage of *in natura* (LR) and nanomodified lettuce roots composite (LR-NP), and 10 mg/L Cr(VI) solution at pH 1.0. $n = 3$

(0.516 mg/g) and LR-NP (0.403 mg/g). The r^2 found for the pseudo-first order model was, respectively, 0.3608 and 0.6918 for LR and LR-NP, and did not describe the data satisfactorily. Thus, the biosorption process was better described by the pseudo-second-order model, which corroborates the assumption that a chemisorption process takes place (Babu et al. 2019).

Sorption capacity and isotherm model parameters

The batch procedure (Fig. S1, Supplementary Material) was used to determine the sorption capacity of the biosorbents. Increasing concentrations of 10 to 100 Cr(VI) mg/L, using magnetite NPs, and LR and LR-NP. All results of this approach are presented in Table 2 and illustrated in Fig. 8. The sorption capacity reached for LR, NP, and LR-NP was 4.51 ± 0.04 mg/g, 2.48 ± 0.57 mg/g, and 3.84 ± 0.08 mg/g, respectively. Although nanomodified biomass presented slightly higher Q_{exp}, nanomodification is desirable to provide easier removal of the biosorbent from the medium by using a magnet to attract the material with superparamagnetic properties.

In addition to biomasses, other materials also have sites available to remove contaminants. Thus, adsorption by iron oxide (NP) occurs mainly due to the hydroxyl groups present on its surface, which tend to vary at different pH values (Hu et al. 2004). Thus, anion adsorption is favored below the point of zero charge of the adsorbent material. At the same time, at higher pHs, there is competition for the sorption sites between hydroxyl ions and Cr(VI) species in the form of chromate. In addition, this difference in the sorption capacity can be attributed to the affinity of magnetite with the different species that coexist at more acidic pHs (Hu et al. 2004).

According to the Giles et al. (1974) classification, the isotherms presented in Fig. 8 are type L, indicating a promising process and demonstrating affinity between adsorbent and adsorbate (Volesky 2004; Limousin et al. 2007). In Table 2, considering the algorithm χ^2 (Labuto et al.2018), it is noted that the presented theoretical models can be satisfactorily applied to the experimental data of Cr(VI) sorption by all adsorbents tested (LR, LR-NP, and NP).

When analyzing the r^2, it was observed that Langmuir, Freundlich, and Sips models presented the best values (0.9628, 0.9580, and 0.9577, respectively) for LR. On the other hand, it is observed that the Q_{max} values provided by Langmuir (9.14 ± 1.6 mg/g) are considerably higher than those found experimentally (4.51 ± 0.04 mg/g). Besides presenting higher Q_{max} than expected (10.29 ± 8.28 mg/g and 9.14 ± 5.75 mg/g, respectively), Sips and Hill models showed unacceptable SE values.

Although the Freundlich model does not predict adsorbent saturation, other parameters, such as n_f, help understand the process since when it presents values between 1 and 10, it indicates that the process occurred favorably (José et al. 2019). In this case, the process was favorable, not only for LR ($n_f = 1.55$) but for the other materials (1.38 and 1.80 for LR-NP and NP, respectively).

When analyzing the D-R model for LR, it is noted that Q_{max} provided by the model was fairly similar to Q_{exp}. However, low r^2 values were found among all the applied models. D-R isotherm provides parameters for calculating free energy (E), allowing a better understanding of the process type: chemosorption and physisorption. For all materials, energy (E) values were low (0.11, 0.10, and 0.08 kJ/mol for NP, LR, and LR-NP, respectively), indicating that sorption exhibits a physical nature as demonstrated by the adjustment of Freundlich's

Table 1 Information of pseudo-first-order kinetics and pseudo-second-order by LR (*in natura* lettuce root biomass), and LR-NP (nanomodified lettuce root biomass), using 100 mg of biosorbent suspended in 10 mL of 100 mg/L Cr(VI) solution. $n = 3$

	Pseudo first order			Pseudo second order		
	r^2	K_1 (min^{-1})	q_{exp} (mg/g)	r^2	K_2 (g/mg min)	q_{exp} (mg/g)
LR	0.3608	0.084	0.1441	0.9982	0.3724	0.5238
LR-NP	0.6918	0.091	0.1876	0.9812	3.77×10^{17}	0.4059

Table 2 Data of experimental sorption capacity (Q_{exp}), isotherms parameters and χ^2 error evaluation for Cr(VI) sorption by magnetic nanoparticles (NP), *in natura* (LR), and nanomodified (LR-NP) lettuce roots. *SD* standard deviation, *SE* standard error provided by fitting the model to the experimental data. $n = 3$

	NP	LR	LR-NP
Q_{exp} (mg/g)	$2.48 \pm 0.57^{(SD)}$	$4.51 \pm 0.04^{(SD)}$	$3.84 \pm 0.08^{(SD)}$
Isotherm model			
Langmuir			
Q_{max} (mg/g)	$3.77 \pm 0.7^{(SE)}$	$9.14 \pm 1.8^{(SE)}$	$8.63 \pm 1.054^{(SE)}$
b (L/g)	$0.0229 \pm 0.0093^{(SE)}$	$0.0164 \pm 0.0056^{(SE)}$	$0.0098 \pm 0.0019^{(SE)}$
r^2	0.9185	0.9628	0.9925
χ^2	0.0721	0.1066	0.0137
Freundlich			
K_f(L/mg)	$0.2185 \pm 0.0971^{(SE)}$	$0.3249 \pm 0.0445^{(SE)}$	$0.16 \pm 0.02^{(SE)}$
n_f	$1.80 \pm 0.36^{(SE)}$	$1.55 \pm 0.18^{(SE)}$	$1.38 \pm 0.07^{(SE)}$
r^2	0.8876	0.9580	0.9909
χ^2	0.0994	0.1202	0.0165
D-R			
Q_{DR}(mg/g)	$2.38 \pm 0.12^{(SE)}$	$4.62 \pm 0.44^{(SE)}$	$3.70 \pm 0.3^{(SE)}$
B_{DR}(mol^2/J^2)	$3.91 \times 10^{-5} \pm 7.7 \times 10^{-6(SE)}$	$4.67 \times 10^{-5} \pm 1.64 \times 10^{-5(SE)}$	$7.39 \times 10^{-5} \pm 1.89 \times 10^{-5(SE)}$
E (kJ/mol)	0.11	0.103	0.08
r^2	0.9471	0.8498	0.9077
χ^2	0.0468	0.43	0.1687
Sips			
Q_{max} (mg/g)	$2.47 \pm 0.25^{(SE)}$	$10.3 \pm 8.28^{(SE)}$	$10.1 \pm 6.63^{(SE)}$
K_s	$0.050 \pm 0.0084^{(SE)}$	$0.013 \pm 0.021^{(SE)}$	$0.007 \pm 0.0088^{(SE)}$
n	$2.12 \pm 0.70^{(SE)}$	$0.93 \pm 0.34^{(SE)}$	$0.94 \pm 0.20^{(SE)}$
r^2	0.9352	0.9577	0.9914
χ^2	0.0574	0.1211	0.0157
Temkin			
b_T	$9.8 \times 10^4 \pm 1.0 \times 10^{4(SE)}$	$6.2 \times 10^4 \pm 7.5 \times 10^{3(SE)}$	$7.1 \times 10^4 \pm 6.8 \times 10^{3(SE)}$
K (L/mg)	$0.18 \pm 0.04^{(SE)}$	$0.30 \pm 0.08^{(SE)}$	$0.19 \pm 0.04^{(SE)}$
r^2	0.9450	0.9194	0.9506
χ^2	0.0487	0.2308	0.0901
Hill			
Q_H (mg/g)	$2.47 \pm 0.25^{(SE)}$	$9.14 \pm 5.75^{(SE)}$	$9.34 \times 10^9 \pm -^{(SE)}$
n_H	$2.12 \pm 0.73^{(SE)}$	$1 \pm 0.35^{(SE)}$	$0.72 \pm 0.041^{(SE)}$
K_H	$565.6 \pm 1152.4^{(SE)}$	$60.95 \pm 27.42^{(SE)}$	$5.747 \times 10^{10} \pm -^{(SE)}$
r^2	0.9352	0.9575	0.9895
χ^2	0.0574	0.1218	0.0193

model. It considers a physical process in multilayers and heterogeneous surfaces (Foo and Hameed 2010).

For the LR-NP, the same isothermal models (Langmuir, Freundlich, and Sips) obtained better adjustments considering r^2 and χ^2. However, the Q_{max} value provided by Langmuir (8.63 ± 1.05 mg/g) was also higher than the experimental (3.84 ± 0.08 mg/g) while Sips, in addition to Q_{max}, also showed a high SE value (10.11 ± 6.63 mg/g).

On the other hand, the Freundlich model indicated that the sorption of Cr(VI) by LR-NP was favorable and with $r^2 = 0.9909$ and $\chi^2 = 0.0165$, presenting an excellent adjustment to the experimental data and indicating that the process is physical, as well as for the LR. It is worth mentioning that the D-R model presented acceptable values of r^2 (0.9076) and χ^2 (0.1687). However, they were not the best, demonstrating to fit well with the experimental data, given the proximity of the Q_{max} value (3.70 ± 0.3 mg/g) to that found experimentally (3.84 ± 0.08 mg/g). Thus, free energy E, calculated by the D-R model, can also indicate that the process is physisorption.

As for NP, the D-R model provides the best r^2 value (0.9471), in addition to Q_{max} (2.38 ± 0.12 mg/g) being very close to the experimental value found (2.48 ± 0.57 mg/g). Considering that the free energy supplied from the B_{DR} parameter is low (0.11 kJ/mol), the process is physical, as suggested for LR and LR-NP. In this way, the Freundlich

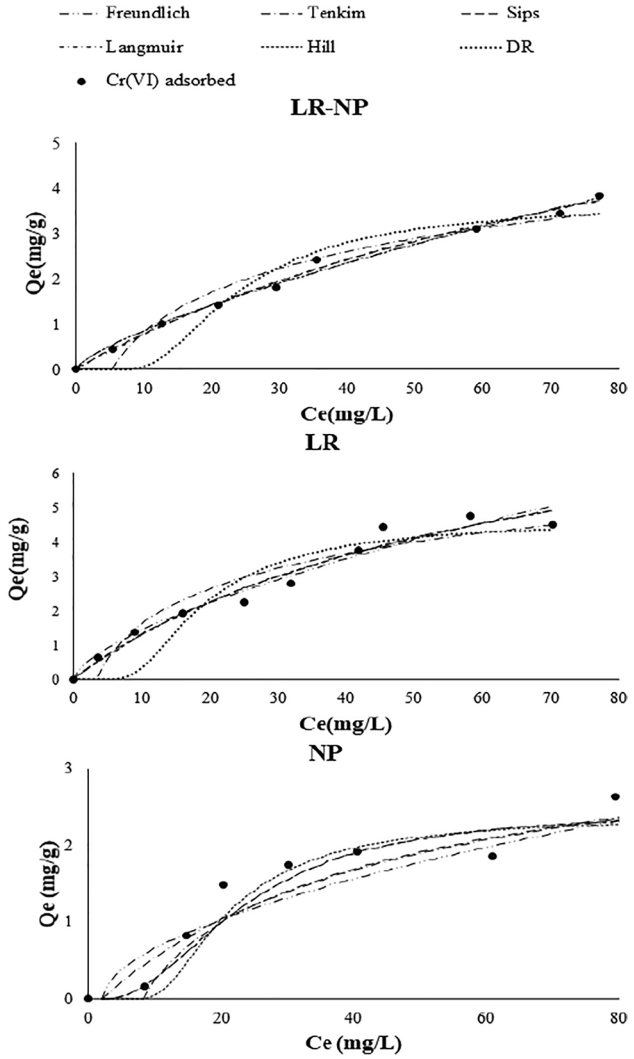

Fig. 8 Isotherms of Cr(VI) sorption by *in natura* (LR) and nanomodified (LR-NP) lettuce roots, using 10–100 mg/L Cr(VI) at pH 1.0, and 30 min contact time. $n = 3$

model can also be adopted to describe the experimental data of Cr(VI) adsorption by NP.

Conclusions

Chromium(VI) sorption by LR and LR-NP proved to be more efficient with decreasing pH, reaching maximum efficiency at pH 1. From the experimental data of sorption kinetics, it was noticed that the process occurs as early as the first 5 min and that equilibrium was reached after 30 min of contact time. The pseudo-second-order model showed a better fit to the experimental data, suggesting that a chemosorption process occurs. Using the previous set parameters pH and kinetics, the sorption capacity studies were performed in 30 min contact time, pH 1.0, and 10 g/L LR and LR-NP dose, so that it was possible to compare the effect of magnetization. Experimental sorption capacity was 4.51 mg/g and 3.84 mg/g for LR and LR-NP, respectively, demonstrating that nanomodification besides facilitating the removal of the metal ion did not reduce sorption capacity significantly. Among the isotherm models applied to experimental data, Freundlich was the model that best described the sorption process by LR, NP, and LR-NP. Therefore, the adsorbent materials proposed in this work are efficient and low-cost alternatives for removing Cr(VI) from water.

Supplementary Information The online version contains supplementary material available at https://doi.org/10.1007/s11356-022-21755-0.

Author contribution EC and GL postulated and supervised the study. BCS and EC planned the experiment. BCS and TEA obtained the data, and EC, GL, and JCJ carried out the data analysis and interpretation. GL performed the adjustment of all experimental data to the isothermal models applied. BCS, JCJ, and TEA prepared the first draft, and EC and GL thoroughly revised the manuscript. EC, GL, and BCS read and approved the final manuscript.

Funding This work was supported by Fundação de Amparo à Pesquisa do Estado de São Paulo (FAPESP) (2016/06271–4 and 2019/08335–8) and Conselho Nacional de Desenvolvimento Científico e Tecnológico (CNPq) (163205/2019–1 and 166783/2019–6).

Availability of data and materials All data generated or analyzed during this study are included in this published article. Extra Data are available from the authors (elma.carrilho@gmail.com) upon reasonable request.

Declarations

Ethical approval Not applicable.

Consent to participate Not applicable.

Consent to publish Not applicable.

Competing interests The authors declare no competing interests.

References

Abilio TE, Soares BC, José JC, Milani PA, Labuto G, Carrilho ENVM (2021) Hexavalent chromium removal from water: adsorption properties of *in natura* and magnetic nanomodified sugarcane bagasse. Environ Sci Pollut Res 28:24816–24829

Akhter MF, Omelon CR, Gordon RA, Moser D, Macfie SM (2014) Localization and chemical speciation of cadmium in the roots of barley and lettuce. Environ Exp Bot 100:10–19

Appel C, Ma LQ, Rhue RD, Kennelley E (2003) Point of zero charge determination in soils and minerals via traditional methods and detection of electroacoustic mobility. Geoderma 113:77–93

Arif Z, Sethy NK, Mishra PK, Verma B (2020) Development of eco-friendly, self-cleaning, antibacterial membrane for the elimination of chromium (VI) from tannery wastewater. Int J Environ Sci Technol 17:4265–4280

Ayawei N, Ebelegi AN, Wankasi D (2017) Modelling and interpretation of adsorption isotherms. J Chem 2017:1–11

Babu DJ, King P, Kumar YP (2019) Optimization of Cu (II) biosorption onto sea urchin test using response surface methodology and artificial neural networks. Int J Environ Sci Te 16:1885–1896

Bakatula EN, Richard D, Neculita CM, Zagury GJ (2018) Determination of point of zero charge of natural organic materials. Environ Sci Pollut Res 25(8):7823–7833

Beretta GZ, Abilio TE, Gabriel L, Labuto G, Carrilho ENVM (2021) Competitive adsorption of Cr(III) and Cr(VI) by sugarcane bagasse magnetic nanocomposite in water matrix: a pH study. Ambiente: Gestão e Desenvolvimento 1(1): 47–54

Binod P, Satyanagalakshmi K, Sindhu R, Janu KU, Sukumaran RK, Pandey A (2012) Short duration microwave assisted pretreatment enhances the enzymatic saccharification and fermentable sugar yield from sugarcane bagasse. Renew Energy 37:109–116

Blaney L (2007) Magnetite (Fe_3O_4): Properties, synthesis, and applications. The Lehigh Review 5(15):33–81

Brito SMO, Cordeiro JLC, Ramalho LC, Oliveira JFR (2019) Eriochrome black adsorption on yellow passion fruit peel (Passiflora edulis f. Flavicarpa) treated with sodium hydroxide and nitric acid: study of adsorption isotherms, kinetic models and thermodynamic parameters. SN Appl Sci 1:1226

Cardona DS, Debs KB, Lemos SG, Vitale G, Nassar NN, Carrilho ENVM, Semensatto D, Labuto G (2019) A comparison study of cleanup techniques for oil spill treatment using magnetic nanomaterials. J Environ Manage 242:362–371

Carvalho JTT, Milani PA, Consonni JL, Labuto G, Carrilho ENVM (2021) Nanomodified sugarcane bagasse biosorbent: synthesis, characterization, and application for Cu(II) removal from aqueous medium. Environ Sci Pollut Res 28:24744–24755

Cid H, Ortiz C, Pizarro J, Moreno-Piraján (2020) Effect of copper (II) biosorption over light metal cation desorption in the surface of macrocystis pyrifera biomass. J Environ Chem Eng 8(3):103729

Conceição JDC, Ramos VHS, Jesus ED, Silva AS, Costa AWMC (2014) Biosorption of Cr(VI) from aqueous solutions using chemically modified okra powder. J Basic Appl Sci 10:73–79

Debs KB, Cardona DS, Silva HDT, Nassar N, Carrilho ENVM, Haddad PS, Labuto G (2019) Oil spill cleanup employing magnetite nanoparticles and yeast-based magnetic bionanocomposite. J Environ Manage 230:405–412

Dhankhar R, Hooda A (2011) Fungal biosorption – an alternative to meet the challenges of heavy metal pollution in aqueous solutions. Environ Technol 32:467–491

Fernández-Nieves A, Richter C, Nieves FJ (1998) Point of zero charge estimation for a TiO_2/water interface. Progr Colloid Polym Sci 110:21–24

Foo KY, Hameed BH (2010) Insights into the modeling of adsorption isotherm systems. Chem Eng J 156:2–10

Furlan FR, Silva LGM, Morgado AF, Souza AAU, Souza SMAGU (2010) Removal of reactive dyes from aqueous solutions using combined coagulation/flocculation and adsorption on activated carbon. Resour Conserv Recycl 54:283–290

Gabriel L, Soares BC, Beretta GZ, Abilio TE, Labuto G, Carrilho ENVM (2021) Effect of pH on the simultaneous sorption of Cr(III) and Cr(VI) by magnetic nanomodified lettuce roots in aqueous medium. Ambiente: Gestão e Desenvolvimento 1(1):19–25

Gadd GM (2009) Biosorption: critical review of scientific rationale, environmental importance and significance for pollution treatment. J Chem Technol Biotechnol 84:13–28

Giles CH, MacEwan TH, Nakhwa SN, Smith D (1960) Studies in adsorption. Part XI. a system of classification of solution adsorption isotherms, and its use in diagnosis of adsorption mechanisms and in measurement of specific surface areas of solids. J Chem Soc 111:3973–3993

Giles CH, Smith D, Huitsom A (1974) A general treatment and classification of the solute adsorption isotherm. I Theoretical J Colloid Interface Sci 47:755–776

Gonzalez M, Araujo G, Pelizaro C, Menezes E, Lemos S, De Souza G, Nogueira A (2008) Coconut coir as biosorbent for Cr(VI) removal from laboratory wastewater. J Hazard Mater 159:252–256

Ho YS (2006) Review of second-order models for adsorption systems. J Hazard Mater 136(3):681–689

Ho YS, Mckay G (2000) The kinetics of sorption of divalent metal ions onto sphagnum moss peat. Water Res 34(3):735–742

Hu J, Lo IMC, Chen G (2004) Removal of Cr(VI) by magnetite nanoparticle. Water Sci Technol 50(12):139–146

Jobby R, Jha P, Kumar A, Desai YN (2018) Biosorption and biotransformation of hexavalent chromium [Cr(VI)]: a comprehensive review. Chemosphere 207:255–266

José JC, Debs KB, Labuto G, Carrilho ENVM (2019) Synthesis, characterization and application of yeast-based magnetic bionanocomposite for the removal of Cu(II) from water. Chem Eng Commun 206(11):1581–1591

Kanagaraj G, Elango L (2019) Chromium and fluoride contamination in groundwater around leather tanning industries in southern India: Implications from stable isotopic ratio $\delta^{53}Cr/\delta^{52}Cr$, geochemical and geostatistical modelling. Chemosphere 220:943–953

Kratochvil D, Pimentel P, Volesky B (1998) Removal of trivalent and hexavalent chromium by seaweed biosorbent. Environ Sci Technol 32:2693–2698

Labuto G, Cardona DS, Debs KB, Imamura AR, Bezerra KCH, Carrilho ENVM, Haddad PS (2018) Low cost agroindustrial biomasses and ferromagnetic bionanocomposites to cleanup textile effluents. Desalin Water Treat 12:80–89

Li J, Ma J, Guo Q, Zhang S, Han H, Zhang S, Han P (2020) Adsorption of hexavalent chromium using modified walnut shell from solution. Water Sci Technol *In press*

Limousin G, Gaudet JP, Charlet L, Szenknect S, Barthes V, Krimissa M (2007) Sorption isotherms: a review on physical bases, modeling and measurement. App Geochem 22:249–275

Liu C, Jin RN, Ouyang XK, Wang YG (2017) Adsorption behavior of carboxylated cellulose nanocrystal–polyethyleneimine composite for removal of Cr(VI) ions. Appl Surf Sci 408:77–87

Milani PA, Consonni JL, Labuto G, Carrilho ENVM (2018a) Agricultural solid waste for sorption of metal ions, part II: competitive assessment in multielemental solution and lake water. Environ Sci Pollut Res 25(36):35906–35914

Milani PA, Debs KB, Labuto G, Carrilho ENVM (2018b) Agricultural solid waste for sorption of metal ions: part I – characterization and use of lettuce roots and sugarcane bagasse for Cu(II), Fe(II), Zn(II), and Mn(II) sorption from aqueous medium. Environ Sci Pollut Res 25(36):35895–35905

Mothé CG, De Miranda IC (2009) Characterization of sugarcane and coconut fibers by thermal analysis and FTIR. J Therm Anal Calorim 97:661–665

Mou B (2008) Lettuce In: Prohens J., Nuez F. Vegetables I. Handbook of Plant Breeding. Springer, New York

Omer AM, Khalifa RE, Hu Z, Zhang H, Liu C, Ouyang XK (2019) Fabrication of tetraethylenepentamine functionalized alginate beads for adsorptive removal of Cr (VI) from aqueous solutions. Int J Biol Macromol 125:1221–1231

Panneerselvam P, Morad N, Tan K (2011) Magnetic nanoparticle (Fe_3O_4) impregnated onto tea waste for the removal of nickel(II) from aqueous solution. J Hazard Mater 186:160–168

Raganati F, Alfe M, Gargiulo V, Chirone R, Ammendola P (2019) Kinetic study and breakthrough analysis of the hybrid physical/chemical CO_2 adsorption/desorption behavior of a magnetite-based sorbent. Chem Eng J 372:526–535

Rossi AD, Rigon MR, Zaparoli M, Braido RD, Colla LM, Dotto GL, Piccin JS (2018) Chromium (VI) biosorption by *Saccharomyces cerevisiae* subjected to chemical and thermal treatments. Environ Sci Pollut Res 25(19):19179–19186

Saadi R, Saadi Z, Fazaeli R, Fard NE (2015) Monolayer and multilayer adsorption isotherm models for sorption from aqueous media. Korean J Chem Eng 32(5):787–799

Santos VC, De Souza JV, Tarley CR, Caetano J, Dragunski DC (2011) Copper ions adsorption from aqueous medium using the biosorbent sugarcane bagasse in natura and chemically modified. Water Air Soil Pollut 216:351–359

Schwantes D, Gonçalves AC Jr, Miola AJ, Coelho GF, Santos MG, Leismann EAV (2015) Removal of Cu (II) and Zn (II) from water with natural adsorbents from cassava agroindustry residues. Acta Sci-Technol 37(3):409–417

Silverstein RM, Webster FX, Kiemle DJ (2012) Spectrometric identification of organic compounds, 8th edn. Wiley, New Jersey

Volesky B (2004) Sorption and Biosorption. BV-Sorbex Inc, St.Lambert, Quebec

Yao Q, Zhang H, WU J, Shao L, He P (2010) Biosorption of Cr(III) from aqueous solution by freeze-dried activated sludge: equilibrium, kinetic and thermodynamic studies. Front Environ Sci Eng China 4(3):286–294

Zheng J-C, Feng H-M, Lam MH-W, Lam PK-S, Ding Y-W, Yu H-Q (2009) Removal of Cu(II) in aqueous media by biosorption using water hyacinth roots as a biosorbent material. J Hazard Mater 171:780–785